

# KERNEL-BASED METHODS FOR NON-LINEAR REDUCED MODELING

P. HÉAS\*, C. HERZET\* , AND B. COMBÈS\*

**Abstract.** An interesting application of kernel-based dynamic mode decomposition (K-DMD) is data-driven reduced modeling of dynamical systems. Such reduced models rely on the solution of low-rank constrained optimization problems defined in reproducing kernel Hilbert spaces (RKHSs). We propose tractable implementations of these reduced models, even though they rely on the optimal solution of infinite-dimensional problems. Particularizing to common kernels, we design low-complexity algorithms going beyond state of the art of non-linear reduced modeling.

**1. Introduction.** Consider a high-dimensional system of the form:

$$\begin{cases} x_t(\theta) = f_t(x_{t-1}(\theta)), & t = 2, \dots, T, \\ x_1(\theta) = \theta, \end{cases} \quad (1.1)$$

where the  $x_t$ 's and  $\theta$ , belonging to  $\mathbb{R}^p$ , constitute respectively a state trajectory and an initial condition, and where  $f_t : \mathbb{R}^p \rightarrow \mathbb{R}^p$  is an arbitrary function whose direct evaluation is considered to be time consuming when  $p$  is large. Among reduced modeling methods, dynamic mode decomposition (DMD) [4, 11, 15] is a popular framework for the approximation of system (1.1). It provides an interesting trade-off between accuracy of the approximation and its computational complexity. Initially designed for linear approximations, DMD has latter been extended to reduced modeling of non-linear behaviors through a decomposition known as extended DMD (EDMD) [12, 16, 17, 18]. In this paper, we will focus on the latter reduced model.

As done in [16, 17], we will presuppose the knowledge of a map  $\Psi : \mathbb{R}^p \rightarrow \mathcal{H}$ , where  $\mathcal{H}$  is a separable Hilbert space endowed with the inner product  $\langle \cdot, \cdot \rangle_{\mathcal{H}}$  and the induced norm  $\| \cdot \|_{\mathcal{H}}$ , such that  $\Psi(x_{t+1}(\theta))$  and  $\Psi(x_t(\theta))$  for  $t = 1, \dots, T-1$  are linearly related by the so-called *Koopman operator* [3, 6, 16]. In this context, reduced modeling consists in building a recursion in  $\mathcal{H}$  of the form

$$\begin{cases} \eta_t(\theta) = \hat{A}_k \eta_{t-1}(\theta), & t = 2, \dots, T, \\ \eta_1(\theta) = \Psi(\theta), \end{cases} \quad (1.2)$$

where  $\hat{A}_k : \mathcal{H} \rightarrow \mathcal{H}$  is a well-chosen linear operator of rank at most  $k$  (satisfying some optimality criterion which will be specified later), yielding an approximation of the state  $x_t(\theta)$  by an inverse mapping<sup>1</sup>

$$\tilde{x}_t(\theta) = \Psi^{-1}(\eta_t(\theta)). \quad (1.3)$$

To obtain a “good” trade-off between accuracy and complexity of the reduced model, one needs to accomplish two challenging tasks: *i*) infer a low-rank operator  $\hat{A}_k$  yielding an accurate approximation of the form (1.2)-(1.3) and *ii*) build a low-complexity algorithm able to compute  $\tilde{x}_t(\theta)$  satisfying recursion (1.2) for a given  $\theta$ .

**Learning  $\hat{A}_k$ .** In this work, the first task is done in a data-driven approach. The training data is a set of representative trajectories  $\{x_t(\vartheta_i)\}_{t=1, i=1}^{T, N}$ , so-called *snapshots*

\*INRIA Centre Rennes - Bretagne Atlantique, campus universitaire de Beaulieu, 35042 Rennes, France (patrick.heas@inria.fr, cedric.herzet@inria.fr, benoit.combes@inria.fr)

<sup>1</sup>A proper definition of the inverse map  $\Psi^{-1}$  will be given in due time.

of the high-dimensional system corresponding to  $N$  initial conditions  $\{\vartheta_i\}_{i=1}^N$ . Using this training data, inspired by the low-rank approximations introduced in [4, 11], we consider a generalization of the minimization problem in [16, 17]. The low-rank operator  $\hat{A}_k$  is the solution of the constrained optimization problem

$$A_k^* \in \arg \min_{A \in \mathcal{B}_k(\mathcal{H}, \mathcal{H})} \sum_{j=1}^{T-1} \sum_{i=1}^N \|\Psi(x_{j+1}(\vartheta_i)) - A\Psi(x_j(\vartheta_i))\|_{\mathcal{H}}^2, \quad (1.4)$$

where  $\mathcal{B}_k(\mathcal{H}, \mathcal{H}) = \{M \in \mathcal{B}(\mathcal{H}, \mathcal{H}) : \text{rank}(M) \leq k\}$  with  $\mathcal{B}(\mathcal{H}, \mathcal{H})$  denoting the class of linear bounded operators from  $\mathcal{H}$  to  $\mathcal{H}$ . In the case where  $\dim(\mathcal{H}) < \infty$ , [7, Theorem 4.1] provides the solution of problem (1.4) for an arbitrary rank  $k$ . In particular, when  $k \geq m$  with  $m = N(T-1)$ , the solution of (1.4) boils down to the least square solution of the unconstrained problem [15]. As detailed in [8], a generalization of [7, Theorem 4.1] to the case of vectors in general Hilbert spaces (*i.e.*, including the case where  $\dim(\mathcal{H}) = \infty$ ) provides a closed-form expression of operator  $A_k^*$  which we will expose in due time.

**Computation of  $\tilde{x}_t(\theta)$ .** State-of-the-art methods propose non-efficient or sub-optimal approaches to compute  $\tilde{x}_t(\theta)$  in (1.3) where we have identified  $\hat{A}_k$  to  $A_k^*$  in recursion (1.2). Indeed, the algorithm designed in [7] for the case where  $\dim(\mathcal{H}) < \infty$  computes the solution  $A_k^*$  with a complexity linear in  $\dim(\mathcal{H})$  and independent of  $t$ . The computation becomes intractable in the case  $\dim(\mathcal{H}) \gg p$ . The large number of dimension of  $\mathcal{H}$  is a recurrent phenomenon for many choices of  $\Psi$ . To overcome this situation, authors in [17] have introduced an approximation of reduced model (1.3) for  $k \geq m$  and for any map  $\Psi$  related to a reproducing kernel Hilbert space (RKHS) [14]. The idea is to rely on the *kernel trick* [2] to compute recursion (1.2) and build approximation (1.3). This algorithm known as kernel-based DMD (K-DMD) enjoys an advantageous complexity linear in  $p$  and independent of  $\dim(\mathcal{H})$ . Unfortunately, as we will detail in the following, it relies on a set of restrictive assumptions which prevents it from reduced modeling in practice.

The main contribution of the present work concerns this second task, *i.e.*, the efficient computation of approximation  $\tilde{x}_t(\theta)$ . We propose a new algorithm dubbed “optimal kernel-based DMD (OK-DMD)” that outperforms and generalizes K-DMD to less restrictive assumptions, while being characterized by the same computational complexity. In particular, we show how to use the optimal (and possibly infinite-dimensional) map  $A_k^*$  given in (1.4) in order to compute exactly the approximation (1.3) with a complexity linear in  $p$  and independent of  $\dim(\mathcal{H})$  and  $t$ . This independence in both, the Hilbert space dimension and the trajectory length, relies on the kernel trick and on the diagonalisation of recursion (1.2). In a nutshell, the kernel trick is used to first recast recursion (1.2) as a linear combination of inner products with eigen-vectors of  $A_k^*$ . It is then used once more for the computation of the inverse mapping from  $\mathcal{H}$  to  $\mathbb{R}^p$  and the obtention of the approximation (1.3).

The paper is organized as follows. After specifying notations, Section 2 specifies the reduced modeling problem of interest and reviews existing sub-optimal solutions. Our generalized kernel-based algorithm is then presented in Section 3 as an optimal solver. The proposed algorithm is evaluated numerically in Section 4. Proofs of theoretical results and technical details are provided in the appendices.

## 2. Problem Statement and State-Of-The-Art.

**2.1. Notations.** We will adopt the following notations. Let  $\mathcal{U}$ ,  $\mathcal{V}$  and  $\mathcal{W}$  be Hilbert spaces.  $\mathcal{B}(\mathcal{V}, \mathcal{U})$  denotes the class of linear bounded operators from  $\mathcal{V}$  to  $\mathcal{U}$ .

The composition of operators  $A \in \mathcal{B}(\mathcal{V}, \mathcal{U})$  and  $B \in \mathcal{B}(\mathcal{W}, \mathcal{V})$  is simply denoted as  $AB \in \mathcal{B}(\mathcal{W}, \mathcal{U})$ . The adjoint of operator  $A$  is denoted  $A^* \in \mathcal{B}(\mathcal{U}, \mathcal{V})$ . Using these notations, operator  $A_k^*$  defined in (1.4) is rewritten as

$$A_k^* \in \arg \min_{A \in \mathcal{B}_k(\mathcal{H}, \mathcal{H})} \|\Psi_{\mathbf{Y}} - A\Psi_{\mathbf{X}}\|_{\mathcal{HS}}^2, \quad (2.1)$$

where operators  $\Psi_{\mathbf{X}}, \Psi_{\mathbf{Y}} \in \mathcal{B}(\mathbb{R}^m, \mathcal{H})$ , with  $m = N(T-1)$ , are defined for any  $w \in \mathbb{R}^m$  as the linear combinations

$$\Psi_{\mathbf{X}}w = \sum_{i,j=1}^{N,T-1} \Psi(x_j(\vartheta_i))w_{(T-1)(i-1)+j} \quad \text{and} \quad \Psi_{\mathbf{Y}}w = \sum_{i,j=1}^{N,T-1} \Psi(x_{j+1}(\vartheta_i))w_{(T-1)(i-1)+j},$$

and where the  $i$ -th component of a vector is denoted by subscript  $i$ .  $\|\cdot\|_{\mathcal{HS}}$  refers to the Hilbert-Schmidt norm, *i.e.*,  $\|\Psi_{\mathbf{Y}} - A\Psi_{\mathbf{X}}\|_{\mathcal{HS}}^2 = \sum_{e_1, \dots, e_m} \|(\Psi_{\mathbf{Y}} - A\Psi_{\mathbf{X}})e_i\|_{\mathcal{H}}^2$ , the  $e_i$ 's being components of an orthonormal basis of  $\mathbb{R}^m$ .

The singular value decomposition (SVD) of operator  $M \in \mathcal{B}(\mathcal{V}, \mathcal{U})$  of rank  $k \leq \dim(\mathcal{V}) \leq \dim(\mathcal{U})$  with  $m = \dim(\mathcal{V}) < \infty$  is denoted  $M = \sum_{i=1}^m \sigma_i^M u_i^M \langle v_i^M, \cdot \rangle_{\mathcal{V}}$ , where  $\{u_i^M\}_{i=1}^m, \{v_i^M\}_{i=1}^m$  are respectively the left and right singular vectors associated to the sequence of decreasing singular values  $\{\sigma_i^M\}_{i=1}^m$  of  $M$ . We use the short-hand SVD notation using operator compositions:  $M = U_M \Sigma_M V_M^*$ , where  $U_M \in \mathcal{B}(\mathbb{C}^m, \mathcal{U})$ ,  $\Sigma_M \in \mathcal{B}(\mathbb{R}^m, \mathbb{R}^m)$  and  $V_M \in \mathcal{B}(\mathcal{V}, \mathbb{C}^m)$  are defined for any vector  $w \in \mathcal{V}$ ,  $s \in \mathbb{C}^m$  as  $U_M s = \sum_{j=1}^m u_j^M s_j$ ,  $(V_M w)_i = \langle v_i^M, w \rangle_{\mathcal{V}}$  and  $(\Sigma_M s)_i = \sigma_i^M s_i$ .

Note that as we have  $m < \infty$ , the SVD of  $M^*M$  boils down to the matrix product  $M^*M = V_M \Sigma_M \Sigma_M V_M^*$  with  $V_M \in \mathbb{C}^{m \times m}$ ,  $\Sigma_M \in \mathbb{R}^{m \times m}$  so that  $V_M^* V_M = I_m$  and  $\Sigma_M$  is diagonal with components  $\sigma_i^M$ . The superscript  $\cdot^*$  denotes in this case the conjugate transpose. The pseudo inverse of  $M$  denoted  $M^\dagger \in \mathcal{B}(\mathcal{U}, \mathcal{V})$  is defined as

$$M^\dagger = \sum_{i=1}^m (\sigma_i^M)^\dagger v_i^M \langle u_i^M, \cdot \rangle_{\mathcal{U}}, \quad \text{where} \quad (\sigma_i^M)^\dagger = \begin{cases} (\sigma_i^M)^{-1} & \text{if } \sigma_i^M > 0 \\ 0 & \text{else} \end{cases},$$

and using short-hand notation  $M^\dagger = V_M \Sigma_M^\dagger U_M^*$ . The orthogonal projector onto the image of  $M$  (resp. of  $M^*$ ) is denoted by  $\mathbb{P}_M = MM^\dagger$  (resp.  $\mathbb{P}_{M^*} = M^\dagger M$ ) [5].

**2.2. The Reduced Modeling Problem.** We are interested in the design of an algorithm computing for any  $\theta \in \mathbb{R}^p$  the approximation  $\tilde{x}_t(\theta)$  using a reduced model of the form of (1.2)-(1.3) where

- $\hat{A}_k$  is identified to  $A_k^*$  defined in (2.1),
- the inverse is defined as the (non necessarily unique) element<sup>2</sup>

$$\Psi^{-1}(\eta) \in \arg \min_{z \in \mathbb{R}^p} \|\eta - \Psi(z)\|_{\mathcal{H}}^2, \quad (2.2)$$

- the algorithm's complexity is independent of both, the Hilbert space dimension  $\dim(\mathcal{H})$  and the trajectory length  $t$ .

---

<sup>2</sup>The definition and the existence of the inverse (2.2) is discussed in Appendix A.

### 2.3. State-Of-The-Art Solutions.

**2.3.1. Low-Rank DMD.** To obtain a low-complexity algorithm, we first assume that  $\hat{A}_k$  is diagonalizable, *i.e.*, there exists an orthonormal basis consisting of eigenvectors of  $\hat{A}_k$ . This assumption will be made all along this work.<sup>3</sup> Thanks to this assumption the complexity needed to evaluate recursion (1.2) becomes independent of the trajectory length  $t$ . Let us make this affirmation explicit. Let  $\{\xi_i\}_{i \in \mathbb{N}}$  and  $\{\zeta_i\}_{i \in \mathbb{N}}$  be bases of  $\mathcal{H}$  associated to the left and right eigen-vectors of  $\hat{A}_k$ , *i.e.*,  $\hat{A}_k \zeta_i = \lambda_i \zeta_i$  and  $\xi_i \hat{A}_k = \lambda_i \xi_i$  for  $i \in \mathbb{N}$ , where  $\{\lambda_i\}_{i \in \mathbb{N}}$  is the related sequence of eigen-values sorted by decreasing absolute values. The finite rank<sup>4</sup> of operator  $\hat{A}_k$  yields the decomposition  $\hat{A}_k \Psi = \sum_{i=1}^k \lambda_i \langle \xi_i, \Psi \rangle_{\mathcal{H}} \zeta_i$ . We see that (1.3) becomes in this case

$$\tilde{x}_t(\theta) = \Psi^{-1} \left( \sum_{i=1}^k \nu_{i,t} \zeta_i \right), \quad \nu_{i,t} = \lambda_i^{t-1} \varphi_i(\theta), \quad (2.3)$$

with  $\varphi_i(\theta) = \langle \xi_i, \Psi(\theta) \rangle_{\mathcal{H}}$ . Note that if  $\Psi^{-1}$  is linear, then (2.3) simplifies to

$$\tilde{x}_t(\theta) = \sum_{i=1}^k \nu_{i,t} \mu_i, \quad \text{with} \quad \mu_i = \Psi^{-1} \zeta_i \in \mathbb{C}^p. \quad (2.4)$$

From (2.3) or (2.4), it is now clear that diagonalizing  $\hat{A}_k$  enables the computation of approximation  $\tilde{x}_t(\theta)$  with a complexity independent of  $t$ . We mention that  $\varphi_i$ 's,  $\mu_i$ 's and  $\lambda_i$ 's are known in the literature respectively as approximations of the  $i$ -th Koopman's *eigen-function*, *eigen-mode* and *eigen-value* [16].

Reduced model (2.3) with the identification  $\hat{A}_k = A_k^*$  is referred to *low-rank EDMD*, while it is called *low-rank DMD* in the particular case where  $\Psi$  is the identity map. In the case where  $\dim(\mathcal{H}) < \infty$ , [7, Theorem 4.1] provides the optimal solution  $A_k^*$  of problem (2.1) for arbitrary value of  $k$ . It can be shown that if  $k \geq m$ , the solution of (2.1) boils down to the solution of the unconstrained problem [15]

$$\hat{A}_k^{\ell s} = \Psi_{\mathbf{Y}} \Psi_{\mathbf{X}}^{\dagger} \quad (2.5)$$

A generalization of [7, Theorem 4.1] to general Hilbert spaces provides a closed-form expression of operator  $A_k^*$  [8]: using the SVD notations to define the operator  $\hat{P} \in \mathcal{B}(\mathbb{R}^k, \mathcal{H}) : w \rightarrow \sum_{i=1}^k u_i^{\mathbf{Z}} w_i$  where  $\mathbf{Z} \in \mathcal{B}(\mathbb{R}^m, \mathcal{H})$  is given by

$$\mathbf{Z} = \Psi_{\mathbf{Y}} \mathbb{P}_{\Psi_{\mathbf{X}}^*}, \quad (2.6)$$

an optimal solution of problem (2.1) for arbitrary value of  $k$  is

$$A_k^* = \hat{P} \hat{P}^* \Psi_{\mathbf{Y}} \Psi_{\mathbf{X}}^{\dagger}. \quad (2.7)$$

Nevertheless, it remains to propose a tractable algorithm to build and evaluate reduced model (2.3) from the closed-form, but potentially infinite-dimensional, optimal solution  $A_k^*$ . In the case where  $\dim(\mathcal{H}) < \infty$ , a straightforward generalization of the algorithm computing low-rank DMD [7, Algorithm 3] to low-rank EDMD involves a complexity linear in  $\dim(\mathcal{H})$ , as long as we are able to evaluate the inverse (2.2) with the same complexity. Even though, the algorithm complexity will not be independent of  $\dim(\mathcal{H})$ , prohibiting its use for  $\dim(\mathcal{H}) \gg p$  or in an infinite-dimensional setting. This straightforward generalization of the low-rank DMD algorithm is thus insufficient for most spaces  $\mathcal{H}$  involved in low-rank EDMD.

<sup>3</sup> This assumption holds in particular if the linear bounded operator  $\hat{A}_k$  is compact self-adjoint or normal [19], or in the case where  $\dim(\mathcal{H}) < \infty$  and all non-zero eigen-values are distinct [10].

<sup>4</sup>  $\hat{A}_k$  has at most  $\text{rank}(\hat{A}_k) \leq k$  non-zero eigen-values.

---

**Algorithm 1** : K-DMD [17]

---

**inputs:** The  $x_t(\vartheta_i)$ 's and a given  $\theta$

- 1) Compute matrices  $\Psi_{\mathbf{X}}^* \Psi_{\mathbf{X}}$ ,  $\Psi_{\mathbf{Y}}^* \Psi_{\mathbf{X}}$  in  $\mathbb{R}^{m \times m}$  and  $\Psi_{\mathbf{X}}^* \Psi(\theta)$  in  $\mathbb{R}^m$  with the kernel trick [2].
  - 2) Get  $(V_{\Psi_{\mathbf{X}}}, \Sigma_{\Psi_{\mathbf{X}}})$  by eigen-decomposition of  $\Psi_{\mathbf{X}}^* \Psi_{\mathbf{X}}$ .
  - 3) Compute the eigen-vectors  $\{\tilde{\xi}_i\}_{i=1}^m$  and eigen-values  $\{\tilde{\lambda}_i\}_{i=1}^m$  of  $R \Psi_{\mathbf{Y}}^* \Psi_{\mathbf{X}} R^*$ , with  $R = \Sigma_{\Psi_{\mathbf{X}}}^\dagger V_{\Psi_{\mathbf{X}}}^*$ .
  - 4) Estimate eigen-functions  $\{\varphi_i(\theta)\}_{i=1}^m$  using (2.9).
  - 5) Compute the pseudo-inverse of  $(\xi_1 \cdots \xi_m)^*$ .
  - 6) Estimate eigen-modes  $\{\mu_i\}_{i=1}^m$  using (2.10).
- output:**  $\hat{x}_t(\theta)$ 's using (2.4) with  $\nu_{i,t} = \tilde{\lambda}_i^{t-1} \varphi_i(\theta)$ .
- 

**2.3.2. K-DMD.** To tackle the high-dimensional setting  $\dim(\mathcal{H}) \gg p$ , authors in [17] propose to relate the map  $\Psi$  to a symmetric, positive definite kernel [2]

$$h : \mathbb{R}^p \times \mathbb{R}^p \rightarrow \mathbb{R}; \quad (y, z) \rightarrow h(y, z) = \langle \Psi(y), \Psi(z) \rangle_{\mathcal{H}}. \quad (2.8)$$

According to the Moore-Aronszajn theorem, there is a unique Hilbert space of functions on  $\mathbb{R}^p$  for which  $h$  is a reproducing kernel. Such a Hilbert space  $\mathcal{H}$  is called an RKHS [14]. The advantage of such a construction is that the kernel trick can be used to compute inner products in the RKHS  $\mathcal{H}$  with a complexity independent of  $\dim(\mathcal{H})$ .

The relation of  $\Psi$  to an RKHS proposed by the authors in [17] results in a tractable algorithm efficient in the case where  $\dim(\mathcal{H}) \gg p$ . This method called K-DMD is detailed in Algorithm 1. Its complexity scales as  $\mathcal{O}(m^2(m+p))$  and is independent of  $\dim(\mathcal{H})$  and  $t$ . The key ideas of K-DMD is on the one hand to use the kernel trick to evaluate inner products with eigen-vectors of the sub-optimal solution (2.5), and on the other hand, to circumvent the intractable computation of the inverse (2.2) by simply assuming that  $\Psi^{-1}$  is linear, so that (2.3) simplifies to (2.4).

Let us describe more precisely this method. First, K-DMD computes matrices in step 1), relying on the kernel-trick. Next, in step 2), 3) and 4), K-DMD relies on the identification of the left eigen-vectors  $\{\xi_i = U_{\Psi_{\mathbf{X}}} \tilde{\xi}_i\}_{i=1}^m$  and eigen-values  $\{\lambda_i = \tilde{\lambda}_i\}_{i=1}^m$  of the sub-optimal solution  $\hat{A}_k^{\ell_s}$ , where  $\{\tilde{\xi}_i\}_{i=1}^m$  and  $\{\tilde{\lambda}_i\}_{i=1}^m$  denote the right eigen-vectors and eigen-values of matrix  $R(\Psi_{\mathbf{Y}}^* \Psi_{\mathbf{X}}) R^* \in \mathbb{R}^{m \times m}$  with  $R = \Sigma_{\Psi_{\mathbf{X}}}^\dagger V_{\Psi_{\mathbf{X}}}^* \in \mathbb{R}^{m \times m}$ . Indeed, as shown latter in Proposition 3.1, the previous identification holds if  $\Psi_{\mathbf{X}}$  is full rank. Using the fact that  $U_{\Psi_{\mathbf{X}}} = \Psi_{\mathbf{X}} R^*$ , a consequence is then that the  $i$ -th eigen-function approximation  $\varphi_i(\theta)$  can be evaluated at any point  $\theta \in \mathbb{R}^p$  as

$$\varphi_i(\theta) = \langle \xi_i, \Psi(\theta) \rangle_{\mathcal{H}} = \tilde{\xi}_i^* R(\Psi_{\mathbf{X}}^* \Psi(\theta)). \quad (2.9)$$

Then, the algorithm approximates the  $\mu_j$ 's in reduced model (2.4). In steps 5) and 6), K-DMD identifies the  $\mu_j$ 's as the minimizers in  $\mathbb{C}^p$  of the square of the  $\ell_2$ -norm of the reduced model error  $\|x_{t+1}(\vartheta_i) - \sum_{j=1}^m \mu_j \lambda_j \langle \xi_j, \Psi(x_t(\vartheta_i)) \rangle_{\mathcal{H}}\|_2^2$  for any data pair  $(x_t(\vartheta_i), x_{t+1}(\vartheta_i))$  satisfying (1.1). We notice that by using (2.9), where  $\Psi(\theta)$  is substituted by  $\Psi(x_t(\vartheta_i))$  for  $i = 1, \dots, N$  and  $j = 1, \dots, T-1$ , we have for  $i = 1, \dots, m$  that

$$(\langle \xi_i, \Psi(x_1(\vartheta_1)) \rangle_{\mathcal{H}} \cdots \langle \xi_i, \Psi(x_{T-1}(\vartheta_N)) \rangle_{\mathcal{H}}) = \tilde{\xi}_i^* \Sigma_{\Psi_{\mathbf{X}}} V_{\Psi_{\mathbf{X}}}^*,$$

The estimated  $\hat{\mu}_j$ 's are thus rewritten as the solution of

$$\arg \min_{\mu_1, \dots, \mu_m} \|\mathbf{Y} - (\mu_1 \cdots \mu_m) \text{diag}(\tilde{\lambda}_1 \cdots \tilde{\lambda}_m) (\tilde{\xi}_1 \cdots \tilde{\xi}_m)^* \Sigma_{\Psi_{\mathbf{X}}} V_{\Psi_{\mathbf{X}}}^*\|_F^2,$$

where  $\|\cdot\|_F$  refers to the Frobenius norm and elements in the set  $\{x_{t+1}(\vartheta_i)\}_{t=1, i=1}^{T-1, N}$  are the columns  $\{y_i\}_{i=1}^m$  of matrix  $\mathbf{Y} \in \mathbb{R}^{p \times m}$ . A minimizer of this least-square optimization problem is

$$(\hat{\mu}_1 \quad \cdots \quad \hat{\mu}_m) = \mathbf{Y} R^* ((\tilde{\xi}_1 \cdots \tilde{\xi}_m)^*)^\dagger \text{diag}(\tilde{\lambda}_1^\dagger \cdots \tilde{\lambda}_m^\dagger). \quad (2.10)$$

Finally, using the identification  $\{\lambda_i = \tilde{\lambda}_i\}_{i=1}^k$ , the  $k$  first eigen-modes estimates  $\{\hat{\mu}_i\}_{i=1}^k$  in (2.10) with the  $\varphi_i(\theta)$ 's given by (2.9) fully parametrize (2.4), yielding the approximation

$$\tilde{x}_t(\theta) = \sum_{i=1}^k \lambda_i^{t-1} \varphi_i(\theta) \hat{\mu}_i. \quad (2.11)$$

However, as proposed in [17], this algorithm computes a rough approximation of reduced model (2.3) in most cases. The lack of optimality of the algorithm originates from : *i*) the assumption that  $\Psi^{-1}$  is linear; *ii*) the assumption that the operator  $\Psi_{\mathbf{X}}$  is full-rank; *iii*) the assumption that the  $\mu_j$ 's belong to the span of  $\mathbf{Y}$ ; *iv*) the substitution of  $A_k^*$  by the sub-optimal solution  $\tilde{A}_k^{\ell s}$ , *i.e.*, the disregard for the low-rank constraint in (2.1).

**3. A Generalized Kernel-Based Algorithm: OK-DMD.** We now detail our generalized kernel-based algorithm called OK-DMD, which computes the low-rank approximation (2.3) with a complexity independent of  $\dim(\mathcal{H})$  and  $t$ . This algorithm is relieved from the restrictive assumptions made in K-DMD. To achieve the design of such an algorithm, we first need to show that the eigen-vectors of operator  $A_k^*$  admit a low-dimensional representation.

**3.1. Eigen-Decomposition of  $A_k^*$ .** Our kernel-based method relies on the following proposition. Let  $\{\xi_i\}_{i=1}^k$  and  $\{\zeta_i\}_{i=1}^k$  denote the left and right eigen-vectors of  $A_k^*$  associated to its at most  $k$  non-zero eigen-values  $\{\lambda_i\}_{i=1}^k$ .

**PROPOSITION 3.1.** *For  $i = 1, \dots, k$ , the left and right eigen-vectors of  $A_k^*$  and its eigen-values satisfy  $\xi_i = U_{\Psi_{\mathbf{X}}} \tilde{\xi}_i$ ,  $\zeta_i = \tilde{P} \tilde{\zeta}_i$  and  $\lambda_i = \tilde{\lambda}_i$  where*

- *$\{(\tilde{\xi}_i, \tilde{\lambda}_i)\}_{i=1}^k$  and  $\{(\tilde{\zeta}_i, \tilde{\lambda}_i)\}_{i=1}^k$  denote respectively the  $k$  right eigen-vectors and (non-zero) eigen-values of the matrices in  $\mathbb{R}^{m \times m}$*

$$(\tilde{A}_{\ell, k})^* = R \Psi_{\mathbf{Y}}^* \Psi_{\mathbf{Y}} S \Psi_{\mathbf{Y}}^* \Psi_{\mathbf{X}} R^*, \quad (3.1)$$

$$\tilde{A}_{r, k} = C \Psi_{\mathbf{Y}}^* \Psi_{\mathbf{Y}} R^* R \Psi_{\mathbf{X}}^* \Psi_{\mathbf{Y}} C^*, \quad (3.2)$$

- *matrices  $S, C \in \mathbb{R}^{m \times m}$  are given by*

$$S = \mathbb{P}_{\Psi_{\mathbf{X}}}^* V_{\mathbf{Z}} \text{diag}((\sigma_{\mathbf{Z}, 1}^\dagger)^2 \cdots (\sigma_{\mathbf{Z}, k}^\dagger)^2 0 \cdots 0) V_{\mathbf{Z}}^* \mathbb{P}_{\Psi_{\mathbf{X}}},$$

$$C = \text{diag}(\sigma_{\mathbf{Z}, 1}^\dagger \cdots \sigma_{\mathbf{Z}, k}^\dagger 0 \cdots 0) V_{\mathbf{Z}}^* \mathbb{P}_{\Psi_{\mathbf{X}}}.$$

Proposition 3.1 gives a decomposition of the left eigen-vectors of the optimal solution  $A_k^*$  given in (2.7). Its proof detailed in Appendix B exploits the factorization of the closed-form solution. We deduce from Proposition 3.1 the closed-form  $i$ -th eigen-function approximation  $\varphi_i(\theta)$  for  $i = 1, \dots, k$  at any point  $\theta \in \mathbb{R}^p$  given in (2.9). Moreover, this proposition provides a closed-form decomposition for the  $\zeta_i$ 's, the right eigen-vectors of  $A_k^*$  and supplies the related eigen-values. Nevertheless, we must be cautious with the normalisation of the eigen-vectors. We verify after some

simple algebraic calculus that the condition  $\langle \xi_i, A_k^* \zeta_i \rangle_{\mathcal{H}} = \lambda_i$  (*i.e.*, the normalisation  $\langle \zeta_i, \xi_i \rangle_{\mathcal{H}} = 1$ ) is ensured if  $\tilde{\zeta}_i$  is rescaled to satisfy  $\zeta_i^* E \tilde{\zeta}_i = 1$ , with

$$E = \Sigma_{\mathbf{Z}}^\dagger V_{\mathbf{Z}}^* \mathbb{P}_{\Psi_{\mathbf{X}}^*} \mathbb{P}_{\Psi_{\mathbf{Y}}^*} \Psi_{\mathbf{Y}}^* \Psi_{\mathbf{X}} R. \quad (3.3)$$

The elements of the set  $\{(\xi_i, \zeta_i, \lambda_i)\}_{i=1}^k$  issued from the eigen-decomposition of  $A_k^*$  correspond to the parameters of the reduced model in (2.3). Relying on the decompositions introduced in Proposition 3.1, the computation of these parameters can be obtained from  $\{(\tilde{\xi}_i, \tilde{\zeta}_i, \tilde{\lambda}_i)\}_{i=1}^k$ . The latter 3-tuple will serve to design a tractable algorithm for the computation of  $\tilde{x}_t(\theta)$ . From now, we already notice that the 3-tuple enables to compute  $\varphi_i(\theta)$ 's using (2.9) and therefore coefficients  $\nu_{i,t}$  in (2.3).

**3.2. Kernel-Based Inversion.** The decomposition of eigen-vectors of  $A_k^*$  provided in Proposition 3.1 constitutes the basic ingredient of the OK-DMD algorithm. However, to achieve the design of this algorithm, it remains to provide a feasible manner to compute  $\Psi^{-1}$  in (2.3). Once more, the idea consists in relying on the kernel trick in order to compute the inverse with a complexity independent of  $\dim(\mathcal{H})$ .

Using Proposition 3.1, we begin by rewriting (2.3) in terms of  $\tilde{\zeta}_i$ 's,  $\varphi_i(\theta)$ 's and  $\tilde{\lambda}_i$ 's as

$$\tilde{x}_t(\theta) = \Psi^{-1} \left( \sum_{j=1}^k \tilde{P} \tilde{\zeta}_j \tilde{\lambda}_j^{t-1} \varphi_j(\theta) \right) = \Psi^{-1} (\Psi_{\mathbf{Y}} g^{\theta,t}), \quad (3.4)$$

with vector

$$g^{\theta,t} = C^* (\tilde{\zeta}_1 \cdots \tilde{\zeta}_k) \begin{pmatrix} \tilde{\lambda}_{\ell,1}^{t-1} \varphi_1(\theta) & \cdots & \tilde{\lambda}_{\ell,k}^{t-1} \varphi_k(\theta) \end{pmatrix}^* \in \mathbb{R}^m.$$

We remark that (3.4) implies the inverse of a linear combination of the  $\Psi(y_i)$ 's, where  $y_i = x_{t+1}(\vartheta_j)$  with  $i = (T-1)j + t$  for  $j = 1, \dots, N$  and  $t = 2, \dots, T$ . Applying definition (2.2), we rewrite the inverse of the linear combination appearing in (3.4) in terms of scalar products in  $\mathcal{H}$  computable using the kernel trick. Given the kernel  $h$  in (2.8), this leads to

$$\tilde{x}_t(\theta) \in \arg \min_{z \in \mathbb{R}^p} \left( h(z, z) - 2 \sum_i g_i^{\theta,t} h(y_i, z) \right). \quad (3.5)$$

The existence of a minimizer (3.5) is shown in Appendix A.2 for the case of polynomial and Gaussian kernels. If a minimizer exists, it can be computed (up to some accuracy) using standard optimization methods with a complexity independent of  $\dim(\mathcal{H})$ . Moreover, the gradient of the objective is in general closed-form, which enables the use of efficient large-scale optimization techniques such as limited memory quasi-newton methods [13]. In this case, the complexity to compute the inverse is linear in  $p$ . Alternatively to solve explicitly problem (3.5), we may use instead a closed-form approximation of the inverse. The approximation uses the assumption of a small magnitude of the columns of  $\mathbf{Y}$ , *i.e.*,  $\|y_i\| \ll 1$ , which holds with an appropriated rescaling of the  $y_i$ 's. We examine the following kernels.

**Polynomial kernels.** Consider the polynomial kernels of the form

$$h(y, z) = (1 + y^* z)^\gamma, \quad \gamma \in \mathbb{N}^*. \quad (3.6)$$

The kernel maps  $\mathbb{R}^p$  onto the RKHS  $\mathcal{H}$  with  $p \leq \dim(\mathcal{H}) < \infty$ . As detailed in Appendix A.3, assuming  $\|y_i\| \ll 1$ , we obtain a closed-form approximation of the inverse of the form

$$\tilde{x}_t(\theta) \approx \mathbf{Y}g^{\theta,t}. \quad (3.7)$$

**Gaussian kernels.** Gaussian kernels of the form

$$h(y, z) = \exp^{-\frac{1}{2\sigma^2}\|y-z\|_2^2}, \quad \sigma > 0, \quad (3.8)$$

map  $\mathbb{R}^p$  onto the RKHS  $\mathcal{H} = L_2(\mathbb{R}^p, \mu)$  where  $\mu$  is a Gaussian measure on  $\mathbb{R}^p$  [14].

As detailed in Appendix A.3, assuming  $\|y_i\| \ll 1$ , we obtain a closed-form approximation of the inverse of the form

$$\tilde{x}_t(\theta) \approx \frac{\mathbf{Y}g^{\theta,t}}{\sum_{i=1}^m g_i^{\theta,t}}. \quad (3.9)$$

**Logarithmic kernel.** Consider a logarithmic kernel defined for vectors  $y, z$  in the set  $\{x \in \mathbb{R}^p : x_i > -1, i = 1, \dots, p\}$  as

$$h(y, z) = (\log(y+1))^* \log(z+1), \quad (3.10)$$

where we have used the short-hand notation

$$\log(y+1)^* = (\log(y_1+1) \cdots \log(y_p+1)).$$

The kernel maps  $x \in \mathbb{R}^p$  onto a vector  $\Psi(x) = \log(x+1) \in \mathbb{R}^p$  so that  $\dim(\mathcal{H}) = p$ . We deduce from definition (3.5) that for entries of  $\mathbf{Y}$  greater than  $-1$  we have a closed-form expression of the  $j$ -th component of  $\tilde{x}_t(\theta)$  given by

$$(\tilde{x}_t(\theta))_j = \prod_{i=1}^m (\mathbf{Y}_{(j,i)} + 1)^{g_i^{\theta,t}} - 1. \quad (3.11)$$

---

#### Algorithm 2 : OK-DMD

---

**inputs:** The  $x_t(\vartheta_i)$ 's and a given  $\theta$

- 1) Compute matrices  $\Psi_{\mathbf{X}}^* \Psi_{\mathbf{X}}$ ,  $\Psi_{\mathbf{Y}}^* \Psi_{\mathbf{Y}}$ ,  $\Psi_{\mathbf{Y}}^* \Psi_{\mathbf{X}}$  in  $\mathbb{R}^{m \times m}$  and  $\Psi_{\mathbf{X}}^* \Psi(\theta)$  in  $\mathbb{R}^m$  with the kernel trick [2].
- 2) Get  $(V_{\Psi_{\mathbf{X}}}, \Sigma_{\Psi_{\mathbf{X}}})$  by eigen-decomposition of  $\Psi_{\mathbf{X}}^* \Psi_{\mathbf{X}}$ .
- 3) Compute  $(V_{\mathbf{Z}}, \Sigma_{\mathbf{Z}})$  by eigen-decomposition of  $\mathbf{Z}^* \mathbf{Z}$  with  $\mathbf{Z}$  given by (2.6).
- 4) Compute matrix  $(\tilde{A}_{\ell,k})^*$  (resp.  $\tilde{A}_{r,k}$ ) given in (3.1) (resp. (3.2)) and compute eigen-vector / eigen-value couples  $\{(\tilde{\xi}_i, \tilde{\lambda}_i)\}_{i=1}^k$  (resp.  $\{(\tilde{\zeta}_i, \tilde{\lambda}_i)\}_{i=1}^k$ ).
- 5) Rescale  $\tilde{\zeta}_i$ 's so that  $\tilde{\zeta}_i E \tilde{\xi}_i = 1$ , with  $E$  given in (3.3).
- 6) Compute eigen-functions  $\{\varphi_i(\theta)\}_{i=1}^k$  using (2.9).
- 7) Compute  $\tilde{x}_t(\theta)$  solving (3.5) or approximate it either with (3.7), (3.9) or (3.11).

**output:**  $\tilde{x}_t(\theta)$ 's.

---

**3.3. The OK-DMD Algorithm.** We have now gathered all the ingredients necessary to design Algorithm 2. As for K-DMD, the OK-DMD exploits the kernel-trick<sup>5</sup> in step 1). However, the main difference with the latter state-of-the-art algorithm is that OK-DMD computes, in the next steps, the exact reduced model (2.3)

---

<sup>5</sup> Let us illustrate the kernel trick with the polynomial kernel (3.6) for  $\gamma = 2$  and  $p = 2$ . Expanding the kernel, we obtain  $h(y, z) = (1 + y^* z)^2 = 1 + 2y_1 z_1 + 2y_2 z_2 + 2y_1 y_2 z_1 z_2 + y_1^2 z_1^2 + y_2^2 z_2^2$ , where  $y = (y_1 \ y_2)^*$  and  $z = (z_1 \ z_2)^*$  in  $\mathbb{R}^2$  so that we have  $h(y, z) = \Psi(y)^* \Psi(z)$ , with  $\Psi(y) = (1 \ \sqrt{2}y_1 \ \sqrt{2}y_2 \ \sqrt{2}y_1 y_2 \ y_1^2 \ y_2^2)^* \in \mathbb{R}^6$ . Therefore, we can evaluate an inner product of vectors in  $\mathcal{H} = \mathbb{R}^6$  by computing a function of an inner product in  $\mathbb{R}^2$ .



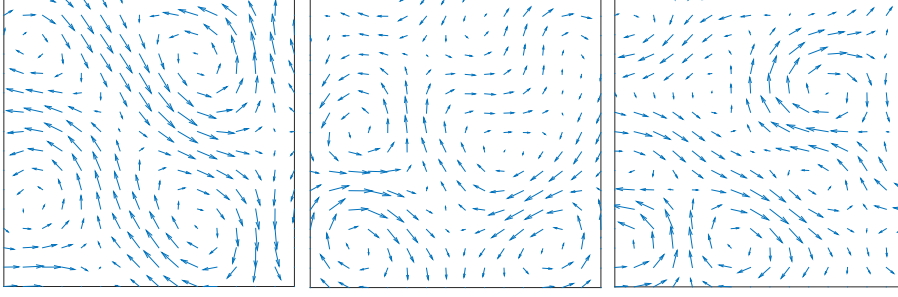


FIG. 4.1. Three examples of snapshot  $x_t(\vartheta_j)$ .

based on the optimal solution (2.7) of problem (2.1). The complexity of the proposed algorithm scales in  $\mathcal{O}(m^2(m+p))$ , just as for K-DMD. We remark that this complexity is independent of  $t$  thanks to the diagonalization of  $A_k^*$ , and independent of  $\dim(\mathcal{H})$  due to the use of the kernel-trick in the first and last steps of the algorithm. The code will be available on-line at <https://gitlab.inria.fr/dmd/matdmd>.

#### 4. Numerical Evaluation.

**4.1. Setup.** The numerical model used for evaluating the respective added-values of the low-rank DMD, K-DMD and OK-DMD algorithms is a synthetic model inspired by the turbulence phenomenology. We set the ambient dimension to  $p = 512$  and the number of snapshots to  $N = 50$ . We draw two independent sets  $\Theta^1 = \{\vartheta_j\}_{j=1}^N$  and  $\Theta^2 = \{\theta_j\}_{j=1}^N$  of initial conditions, used respectively for training and testing the methods. Each initial condition  $\vartheta_j \in \mathbb{R}^p$  (or  $\theta_j \in \mathbb{R}^p$ ) is a sample from a bi-variate bi-dimensional divergence-free fractional Brownian motion field of Hurst exponent  $1/3$ . The samples are drawn using the fractional wavelet representation proposed in [9, Proposition 3.1] with 18 coefficients. Each initial condition is corrupted by an additional Gaussian white noise of standard deviation of  $10^{-6}$ . Each snapshot in  $\{x_t(\vartheta_j)\}_{j=1, t=1}^{N, T}$  or  $\{x_t(\theta_j)\}_{j=1, t=1}^{N, T}$  is a motion field defined on a grid of size  $\sqrt{p/2} \times \sqrt{p/2}$  satisfying (1.1) the quadratic model

$$f(x_t) = (x_{t-1} + 1)^2 + \alpha L x_{t-1} - 1, \quad (4.1)$$

where the square power is taken component-wise, the diffusion coefficient is  $\alpha = 0.5$  and  $L \in \mathbb{R}^{p \times p}$  is a second order finite difference approximation of the (bi-variate) two-dimensional Laplacian operator. We set  $T = 2$ , i.e.,  $m = N$ . Examples of snapshots are presented in Figure 4.1. We mention that the  $\vartheta_j$ 's are rescaled so that  $\|x_2(\vartheta_j)\| \sim 1.e - 2$ , i.e., implying a good agreement with the condition  $\|y_i\| \ll 1$  as required by approximations (3.7) and (3.9)

We assess the gain in performance brought by learning the reduced model with OK-DMD instead of using the state-of-the-art K-DMD or the low-rank DMD algorithm. The reduced model is learnt using snapshots generated with the set of initial conditions  $\Theta^1$ . We analyze the normalized error norms

$$\epsilon(\Theta^1) = \left( \frac{\sum_{j=1}^N \|\tilde{x}_2(\vartheta_j) - x_2(\vartheta_j)\|_2^2}{\sum_{j=1}^N \|x_2(\vartheta_j)\|_2^2} \right)^{1/2} \quad \text{and} \quad \epsilon(\Theta^2) = \left( \frac{\sum_{j=1}^N \|\tilde{x}_2(\theta_j) - x_2(\theta_j)\|_2^2}{\sum_{j=1}^N \|x_2(\theta_j)\|_2^2} \right)^{1/2},$$

where  $x_2(\vartheta_j)$ 's and  $x_2(\theta_j)$ 's are snapshots computed with (1.1) and their approximations  $\tilde{x}_2(\vartheta_j)$ 's and  $\tilde{x}_2(\theta_j)$ 's are computed with (3.5) or its approximations for OK-

DMD, with (2.11) for K-DMD or using the low-rank DMD algorithm [7, Algorithm 3]. The criterion  $\epsilon(\Theta^1)$  evaluates the capability of the reduced model to reproduce the snapshots belonging to the training data set associated to  $\Theta^1$ , while  $\epsilon(\Theta^2)$  reveals its aptitude to predict new snapshots of an independent data set, associated to the initial conditions in  $\Theta^2$ .

**4.2. Results.** Figure 4.2 plots the approximation error as a function of the reduced model dimension, for different choices of kernel. Error curves correspond either to the polynomial kernel (3.6) with  $\gamma = 2$ , the Gaussian kernel (3.8) with  $\sigma = 100$  or the logarithmic kernel (3.10).

**4.2.1. Training.** We first focus on the training context, *i.e.*, we learn the reduced model and evaluate its performance using the same set  $\Theta^1$  of initial conditions. The error criterion is in this case  $\epsilon(\Theta^1)$ .

The left plots of Figure 4.2 show that low-rank DMD or OK-DMD perform pretty good in comparison to K-DMD. The gain compared to K-DMD is more than a decade for  $k \in [14, 48]$ . Moreover, the error curves of the two most accurate methods are very close except in the case where OK-DMD uses a polynomial kernel, which is apparently not suited for the reduction of the dynamics (4.1). The gain in accuracy between K-DMD and OK-DMD can be interpreted as the fact that the OK-DMD algorithm computes exactly reduced model (2.3), *i.e.*, considers the low-rank constraint in problem (2.1) and avoids making the least-square approximation (2.10).

We observe that the three methods yield the same vanishing error in the situation where  $k = m$ , *i.e.*, the dimension of the reduced model corresponds to the number of snapshots used for training. The agreement of K-DMD and OK-DMD at this coordinate is expected: we know that  $\Psi_{\mathbf{X}}$  is full rank, that  $\Psi^{-1}$  is well approximated by a linear function (as shown in (3.7) and (3.9)), which in turns implies that the span of the  $\mu_i$ 's is in the span of the columns of  $\mathbf{Y}$ ; finally, we know that at the coordinate  $k = m$ , the low rank constraint is inactive. The error at this point vanishes since in this training context, the  $x_2(\vartheta_j)$ 's are at the same time the columns of  $\mathbf{Y}$  and the test data.

The OK-DMD results are influenced by the choice of kernel. In particular, the logarithmic kernel seems to be the most performant, the Gaussian kernels performs almost as good, while the polynomial kernel is apparently not appropriated. The following explanation can light up the good performance of the logarithmic kernel. In the case  $\alpha = 0$  (non diffusive model), we note that the logarithmic kernel maps the non-linear dynamics (4.1) into a linear one. Therefore, if the linear model in the induced RKHS concentrates the features in some low-dimensional subspace, we should obtain with this kernel a “good” approximation. For a diffusive model ( $\alpha > 0$ ), the dynamics in the RKHS is no longer linear, but is still well-approximated according to the curves of Figure 4.2. Beyond the focus of the present work, we mention that the optimal choice of mapping is an open question which raises a surge of interest, see for example [18, 12].

The sudden decrease around  $k = 14$  of the OK-DMD and low-rank DMD errors reveals an approximate intrinsic dimension of the snapshots, which is slightly smaller than the dimension of the noise-free initial condition (18 independent wavelet coefficients), suggesting a dynamics contracting trajectories.

**4.2.2. Testing.** We then turn to the evaluation of the predictive capability of the reduced models, *i.e.*, we learn the reduced model using initial conditions in  $\Theta^1$  and evaluate its performance for the independent set  $\Theta^2$ . The error criterion is in this

case  $\epsilon(\Theta^2)$ .

As expected, the right plots of Figure 4.2 show that OK-DMD is everywhere more or as accurate than K-DMD. The gain in accuracy between the two algorithms reaches two decades for the Gaussian kernel in the range  $k \in [14, 48]$ . The two kernel-based algorithms yield identical result around  $k = m$ , which suggests that the K-DMD assumptions all hold in this case. Nevertheless, on the contrary to the training setting, the error does not entirely vanish at this point since the test data, *i.e.*, the  $x_2(\theta_j)$ 's do not belong to the span of the  $\mu_i$ 's.

Additionally, we observe that OK-DMD is more accurate than low-rank DMD for  $k > 14$ , *i.e.*, greater than the approximate intrinsic dimension of snapshots. Nearly two decades separate the two curves. Indeed, the OK-DMD continually reduces the error as  $k$  increases. Low-rank DMD achieves the same level of accuracy up to  $k = 14$ . Increasing the number of components of the reduced model does not improve (and actually even deteriorates) accuracy for  $k > 15$ . This means that the 14 first learned components of the dynamics describe both, the training and the testing data set, while the other learned components are useless to describe snapshots of the testing data set.

Besides, as for the training setting, we note that the relative performance of the kernels is preserved : logarithmic or Gaussian kernels perform the best while the polynomial kernel does not manage to reduce significantly the dynamics for  $k \geq 15$ .

Finally, we proceed to a visual inspection of the error maps. Figure 4.3 displays a typical error map  $\tilde{x}_2(\theta_j) - x_2(\theta_j)$ , where  $\tilde{x}_2(\theta_j)$  denotes the approximation produced the algorithms using a particular initial condition  $\theta_j \in \Theta^2$ . Interestingly, we observe that the large vortices of the flow are correctly approximated by OK-DMD for  $k = 16$ . The only structures that OK-DMD does not reconstruct accurately are the small vortices of the divergence-free fBm. Although low-rank DMD produces a reasonable error, we remark that low-rank DMD clearly fails in identifying some of the large structures of the flow. The inspection of the large error produced by K-DMD at  $k = 16$ , taking exactly the form of the opposite of the snapshot's largest vortices, confirms its poor capabilities for reduced modeling.

**5. Conclusion.** This work presents an algorithm for data-driven non-linear reduced modeling. Using kernel-based computation, the algorithm learns from the snapshots a low-dimensional representation of the eigen-vectors of a linear low-rank operator characterizing the dynamics projected onto a RKHS. The proposed OK-DMD algorithm enhances state-of-the-art by solving with a comparable computational cost, the non-linear reduced model problem in a general setting. A numerical evaluation illustrates the gain brought by the proposed algorithm.

## Appendix A. Inverse Mapping.

**A.1. Definition.** Assume that  $\Psi^{-1}$  maps any element of the subset  $\mathcal{S} = \{x \in \mathcal{H} : x = \Psi(y), y \in \mathbb{R}^p\} \subseteq \mathcal{H}$  to a unique element of  $\mathbb{R}^p$ . We show hereafter that this holds if  $\mathcal{H}$  is a RKHS, due to the kernel properties. Noticing that the definition of the inverse can be interpreted as a minimizer of a distance in the RKHS, we then extend this definition to any element of  $\mathcal{H}$ . However, in general, uniqueness nor even existence is guaranteed outside of  $\mathcal{S}$ . These issues are discussed in Section A.2.

The positive-definiteness of  $h$  implies we have for any  $y, z \in \mathbb{R}^p$

$$\det \begin{pmatrix} h(y, y) & h(y, z) \\ h(z, y) & h(z, z) \end{pmatrix} \geq 0,$$

and the lower bound is reached if and only if  $y = z$ . Using the kernel symmetry, this is equivalent to

$$\frac{h(y, z)^2}{h(y, y)h(z, z)} = \frac{\langle \Psi(y), \Psi(z) \rangle_{\mathcal{H}}^2}{\|\Psi(y)\|_{\mathcal{H}}^2 \|\Psi(z)\|_{\mathcal{H}}^2} \leq 1, \quad (\text{A.1})$$

for any  $y, z \in \mathbb{R}^p$  where the upper bound is reached if and only if  $y = z$ . Therefore, for any  $\eta \in \mathcal{S}$ ,  $\Psi^{-1}(\eta)$  is the unique element of  $\mathbb{R}^p$  given by

$$\Psi^{-1}(\eta) = \arg \max_{z \in \mathbb{R}^p} \frac{\langle \eta, \Psi(z) \rangle_{\mathcal{H}}}{\|\Psi(z)\|_{\mathcal{H}}}. \quad (\text{A.2})$$

Now, can we extend the definition (A.2) outside of  $\mathcal{S}$ ? As defined in (2.2), the inverse of any  $\eta$  in  $\mathcal{H}$  is an element of  $\mathbb{R}^p$  satisfying

$$\Psi^{-1}(\eta) \in \arg \min_{z \in \mathbb{R}^p} \|\eta - \Psi(z)\|_{\mathcal{H}}^2.$$

We notice that definition (2.2) coincides with definition (A.2) for normalized kernels (or more generally if  $\|\Psi(z)\|_{\mathcal{H}} = \text{cte}$ ) for any  $\eta$  in  $\mathcal{S}$ . However, it is not clear if this inverse exists outside of  $\mathcal{S}$  or for non-normalized kernels. This existence is discussed in Appendix A.2.

**A.2. Existence.** We want to show the existence of the inverse as defined in (2.2) for any linear combination  $\eta = \sum_i^m g_i^{\theta, t} \Psi(y_i)$  of elements  $\Psi(y_i)$  of  $\mathcal{S}$ . This is equivalent to show that there exists a vector  $z^* \in \mathbb{R}^p$  satisfying

$$\|\Psi(z^*)\|_{\mathcal{H}} - 2\langle \eta, \Psi(z^*) \rangle_{\mathcal{H}} = \inf_{z \in \mathbb{R}^p} f(z),$$

with  $f(z) = h(z, z) - 2\sum_i^m g_i^{\theta, t} h(y_i, z)$ . The Weierstrass' Theorem [1, Proposition A.8] states that if the domain is non-empty and closed (which is the case for  $\mathbb{R}^p$ ) and the objective function is coercive and lower semicontinuous on  $\mathbb{R}^p$ , then the infimum exists.

- In the case of polynomial kernels,  $f(z)$  is continuous. It remains to show that

$$f(z) = (1 + \|z\|^2)^\gamma - 2 \sum_i^m g_i^{\theta, t} (1 + z^* y_i)^\gamma,$$

is coercive. Letting the magnitude of any component  $z_j$  of  $z$  grow to infinity, we check that

$$\lim_{|z_j| \rightarrow \infty} f(z) = \lim_{|z_j| \rightarrow \infty} \|z\|^{2\gamma} = +\infty,$$

- For Gaussian kernel,  $f(z)$  is continuous. Moreover, we observe that

$$\begin{aligned} \inf_{z \in \mathbb{R}^p} f(z) &= \inf_{z \in \mathbb{R}^p} \left( - \sum_i^m g_i^{\theta, t} e^{-\frac{1}{2\sigma^2} \|y_i - z\|_2^2} \right), \\ &= \inf_{z \in \mathbb{R}^p} -\log \left( \sum_i^m g_i^{\theta, t} e^{-\frac{1}{2\sigma^2} \|y_i - z\|_2^2} \right). \end{aligned} \quad (\text{A.3})$$

It remains to show that the objective in (A.3) is coercive. Letting magnitude of any component  $z_j$  of  $z$  grow to infinity, we have

$$\lim_{|z_j| \rightarrow \infty} f(z) = \lim_{|z_j| \rightarrow \infty} -\log \left( \sum_i^m g_i^{\theta, t} e^{-\frac{1}{2\sigma^2} \|y_i - z\|_2^2} \right) = +\infty. \quad (\text{A.4})$$

### A.3. Closed-Form Approximations.

- For polynomial kernels, using the binomial Theorem yields

$$f(z) = (1 + \|z\|^2)^\gamma - 2 \sum_{i=1}^m g_i^{\theta,t} \sum_{k=0}^{\gamma} \binom{\gamma}{k} (z^* y_i)^k.$$

Assuming that the  $y_i$ 's are small, *i.e.*,  $\|y_i\| \ll 1$ , using a Taylor expansion, we obtain a first-order approximation of  $f(z)$  of the form

$$f(z) \approx (1 + \|z\|^2)^\gamma - 2 \sum_{i=1}^m g_i^{\theta,t} \left( 1 + \frac{\gamma!}{(\gamma-1)!} (z^* y_i) \right).$$

Cancelling the derivative of  $f(z)$  yields

$$z(1 + \|z\|^2)^{\gamma-1} = \sum_{i=1}^m g_i^{\theta,t} y_i. \quad (\text{A.5})$$

Since  $(1 + \|z\|^2)^{\gamma-1} \geq 1$ , using again the assumption that  $\|y_i\| \ll 1$ , we obtain

$$\|z\| \leq \left\| \sum_{i=1}^m g_i^{\theta,t} y_i \right\| \leq \sum_{i=1}^m |g_i^{\theta,t}| \|y_i\| \ll \sum_{i=1}^m |g_i^{\theta,t}|.$$

If in addition the condition  $\sum_{i=1}^m |g_i^{\theta,t}| \ll \infty$  holds, then  $\|z\| \ll 1$  and  $(1 + \|z\|^2)^{\gamma-1} \approx 1$ . It follows from (A.5) that

$$\inf_{z \in \mathbb{R}^p} f(z) \approx \sum_{i=1}^m g_i^{\theta,t} y_i.$$

- For Gaussian kernels, assuming that the  $y_i$ 's are small, *i.e.*,  $\|y_i\| \ll 1$ , using a Taylor expansion, we obtain a first-order approximation of  $f(z)$  of the form

$$\inf_{z \in \mathbb{R}^p} f(z) \approx \inf_{z \in \mathbb{R}^p} - \sum_{i=1}^m g_i^{\theta,t} \left( 1 - \frac{1}{2\sigma^2} \|y_i - z\|_2^2 + \sum_{k=2}^{\infty} \frac{(-\frac{1}{2\sigma^2})^k z^{2k}}{k!} \right).$$

Cancelling the derivative of  $f(z)$  yields

$$z \sum_{i=1}^m g_i^{\theta,t} \left( e^{-\frac{1}{2\sigma^2} \|z\|_2^2} + \frac{\|z\|_2^2}{2\sigma^2} \right) = \sum_{i=1}^m g_i^{\theta,t} y_i. \quad (\text{A.6})$$

Since we have  $(e^{-\frac{1}{2\sigma^2} \|z\|_2^2} + \frac{\|z\|_2^2}{2\sigma^2}) \geq 1$ , it follows that

$$\|z\| \leq \left\| z \sum_{i=1}^m \frac{g_i^{\theta,t}}{\sum_{i'=1}^m g_{i'}^{\theta,t}} \left( e^{-\frac{1}{2\sigma^2} \|z\|_2^2} + \frac{\|z\|_2^2}{2\sigma^2} \right) \right\| = \left\| \sum_{i=1}^m \frac{g_i^{\theta,t}}{\sum_{i'=1}^m g_{i'}^{\theta,t}} y_i \right\| \leq \sum_{i=1}^m \left| \frac{g_i^{\theta,t}}{\sum_{i'=1}^m g_{i'}^{\theta,t}} \right| \|y_i\|$$

In addition if the condition  $\sum_{i=1}^m \left| \frac{g_i^{\theta,t}}{\sum_{i'=1}^m g_{i'}^{\theta,t}} \right| \ll \infty$  holds, we deduce from the assumption  $\|y_i\| \ll 1$  that  $\|z\| \ll 1$  and that  $(e^{-\frac{1}{2\sigma^2} \|z\|_2^2} + \frac{\|z\|_2^2}{2\sigma^2}) \approx 1$ . We then deduce from (A.6) that

$$\inf_{z \in \mathbb{R}^p} f(z) \approx \frac{\sum_{i=1}^m g_i^{\theta,t} y_i}{\sum_{i=1}^m g_i^{\theta,t}}.$$

Finally, it is straightforward to show that  $\sum_{i=1}^m |g_i^{\theta,t}| \ll \infty$  or  $\sum_{i=1}^m |\frac{g_i^{\theta,t}}{\sum_{i'=1}^m g_{i'}^{\theta,t}}| \ll \infty$  holds as long as  $\|\theta\| \ll \infty$ ,  $\|x_i\| \ll \infty$  and  $\|y_i\| \ll \infty$  for  $i = 1, \dots, m$ .

**Appendix B. Proof of Proposition 3.1.** We know that the closed-form solution (2.1) is  $A_k^* = \hat{P}\hat{P}^*\Psi_Y\Psi_X^\dagger$  [8].

We begin by proving that the  $U_{\Psi_X}\tilde{\xi}_i$ 's are right eigen-vectors of  $(A_k^*)^*$ . Using (3.1), we verify after some algebraic manipulations that  $U_{\Psi_X}^*(A_k^*)^*U_{\Psi_X} = (\tilde{A}_{\ell,k})^*$ . Besides, exploiting the SVD of  $\Psi_X$ , we have  $(A_k^*)^* = U_{\Psi_X}\Sigma_{\Psi_X}^\dagger V_{\Psi_X}^*\Psi_Y^*\hat{P}\hat{P}^*$ . This leads to  $(A_k^*)^*U_{\Psi_X}\beta = U_{\Psi_X}(\tilde{A}_{\ell,k})^*\beta$ , for any  $\beta \in \mathbb{R}^m$ . By setting  $\beta = \tilde{\xi}_i$  and exploiting the fact that  $(\tilde{\xi}_i, \tilde{\lambda}_i)$  are couples of eigen-vectors and eigen-values of  $(\tilde{A}_{\ell,k})^*$ , we get for  $i = 1, \dots, k$  that  $(A_k^*)^*U_{\Psi_X}\tilde{\xi}_i = U_{\Psi_X}(\tilde{A}_{\ell,k})^*\tilde{\xi}_i = \tilde{\lambda}_i U_{\Psi_X}\tilde{\xi}_i$ , which proves that  $U_{\Psi_X}\tilde{\xi}_i$  and  $\tilde{\lambda}_i$  are eigen-vectors and eigen-values of  $(A_k^*)^*$ .

We continue by showing that the  $\hat{P}\tilde{\zeta}_i$ 's are right eigen-vectors of  $A_k^*$ . It straightforward to verify that  $\hat{P}^*A_k^*\hat{P} = \tilde{A}_{r,k}$ , yielding that  $A_k^*\hat{P}\beta = \hat{P}\tilde{A}_{r,k}\beta$ , for any  $\beta \in \mathbb{R}^m$ . Because  $\tilde{\zeta}_i$  are eigen-vectors of  $\tilde{A}_{r,k}$ , we deduce from the previous relation that  $A_k^*\hat{P}\tilde{\zeta}_i = \hat{P}\tilde{A}_{r,k}\tilde{\zeta}_i = \tilde{\lambda}_i\hat{P}\tilde{\zeta}_i$ , for  $i = 1, \dots, k$ . This proves that the  $\hat{P}\tilde{\zeta}_i$ 's and the  $\tilde{\lambda}_i$ 's are right eigen-vectors and eigen-values of  $A_k^*$ .

## REFERENCES

- [1] Bertsekas, D.: Nonlinear Programming. Athena Scientific (1995)
- [2] Bishop, C.M.: Pattern Recognition and Machine Learning (Information Science and Statistics). Springer-Verlag, Berlin, Heidelberg (2006)
- [3] Budišić, M., Mohr, R., Mezić, I.: Applied koopmanism a. Chaos: An Interdisciplinary Journal of Nonlinear Science **22**(4), 047,510 (2012)
- [4] Chen, K.K., Tu, J.H., Rowley, C.W.: Variants of dynamic mode decomposition: boundary condition, koopman, and fourier analyses. Journal of nonlinear science **22**(6), 887–915 (2012)
- [5] Golub, G., Van Loan, C.: Matrix Computations. Johns Hopkins Studies in the Mathematical Sciences. Johns Hopkins University Press (2013)
- [6] Goswami, D., Thackray, E., Paley, D.A.: Constrained ulam dynamic mode decomposition: Approximation of the perron-frobenius operator for deterministic and stochastic systems. IEEE Control Systems Letters **2**, 809–814 (2018)
- [7] Héas, P., Herzet, C.: Low rank dynamic mode decomposition: Optimal solution in polynomial time. arXiv e-prints (2017)
- [8] Héas, P., Herzet, C.: Low-rank approximation of linear maps. arXiv e-prints (2018)
- [9] Héas, P., Lavancier, F., Kadri-Harouna, S.: Self-similar prior and wavelet bases for hidden incompressible turbulent motion. SIAM Journal on Imaging Sciences **7**(2), 1171–1209 (2014)
- [10] Horn, R.A., Johnson, C.R.: Matrix analysis. Cambridge university press (2012)
- [11] Jovanovic, M., Schmid, P., Nichols, J.: Low-rank and sparse dynamic mode decomposition. Center for Turbulence Research Annual Research Briefs pp. 139–152 (2012)
- [12] Lusch, B., Kutz, J.N., Brunton, S.L.: Deep learning for universal linear embeddings of nonlinear dynamics. In: Nature Communications (2018)
- [13] Nocedal, J., Wright, S.: Numerical Optimization. Springer Series in Operations Research and Financial Engineering. Springer New York (2000)
- [14] Steinwart, I., Hush, D., Scovel, C.: An explicit description of the reproducing kernel hilbert spaces of gaussian rbf kernels. IEEE Transactions on Information Theory **52**(10), 4635–4643 (2006)
- [15] Tu, J.H., Rowley, C.W., Luchtenburg, D.M., Brunton, S.L., Kutz, J.N.: On dynamic mode decomposition: Theory and applications. Journal of Computational Dynamics **1**(2), 391–421 (2014)
- [16] Williams, M.O., Kevrekidis, I., Rowley, C.: A data-driven approximation of the koopman

- operator: Extending dynamic mode decomposition. *Journal of Nonlinear Science* **25**(6), 1307–1346 (2015)
- [17] Williams, M.O., Rowley, C.W., Kevrekidis, I.G.: A kernel-based method for data-driven koopman spectral analysis. *Journal of Computational Dynamics* **2**(2), 247–265 (2015)
  - [18] Yeung, E., Kundu, S., Hodos, N.: Learning deep neural network representations for koopman operators of nonlinear dynamical systems. *arXiv preprint arXiv:1708.06850* (2017)
  - [19] Zhu, K.: *Operator Theory in Function Spaces*, Second Edition. *Mathematical surveys and monographs*. American Mathematical Soc. (2007)

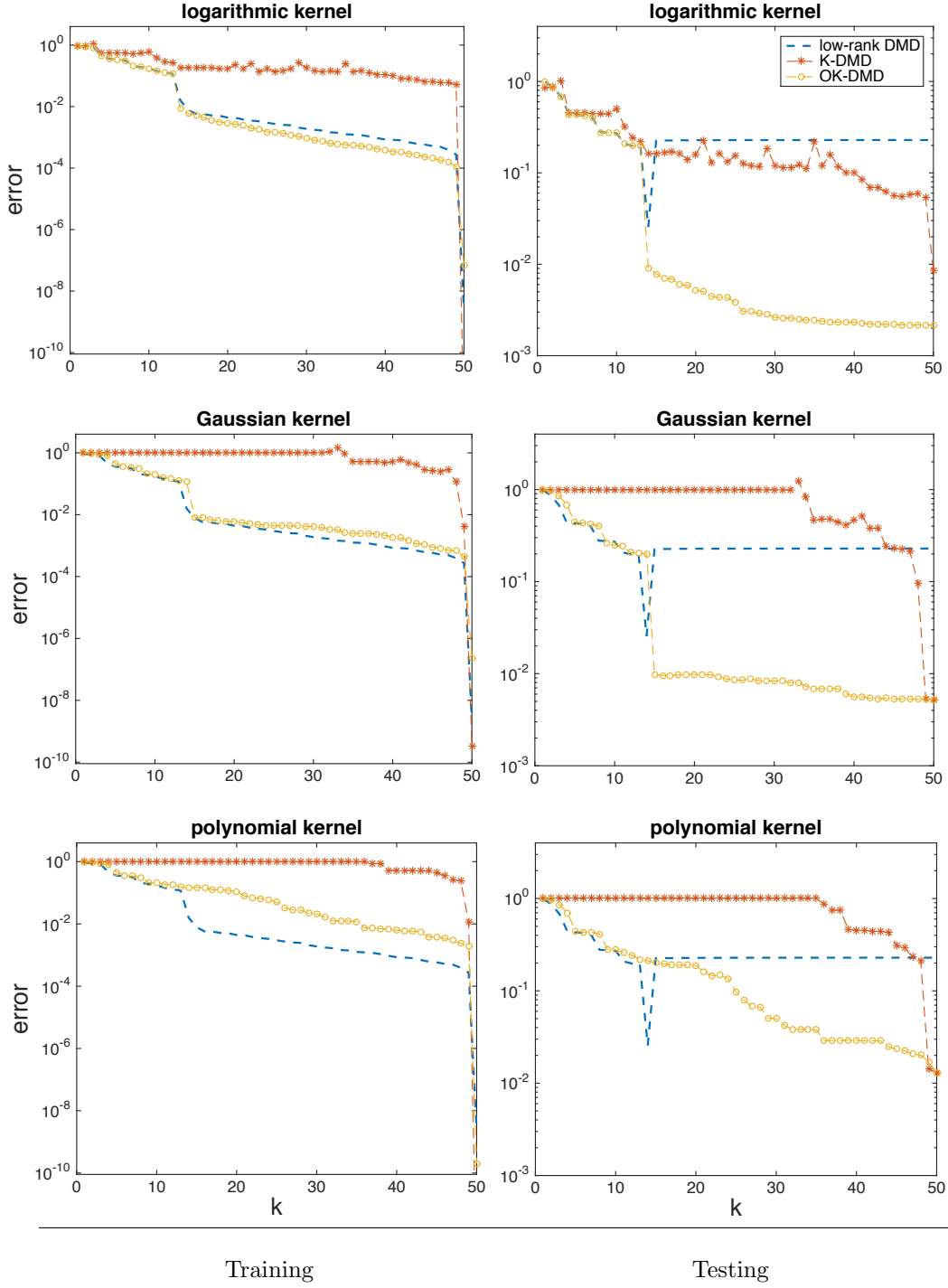


FIG. 4.2. Evaluation of reduced model approximation error. Evaluation of errors  $\epsilon(\Theta^1)$  (left) and  $\epsilon(\Theta^2)$  (right) as a function of the dimension  $k$  of the reduced-model approximation, for logarithmic, Gaussian or polynomial kernels.



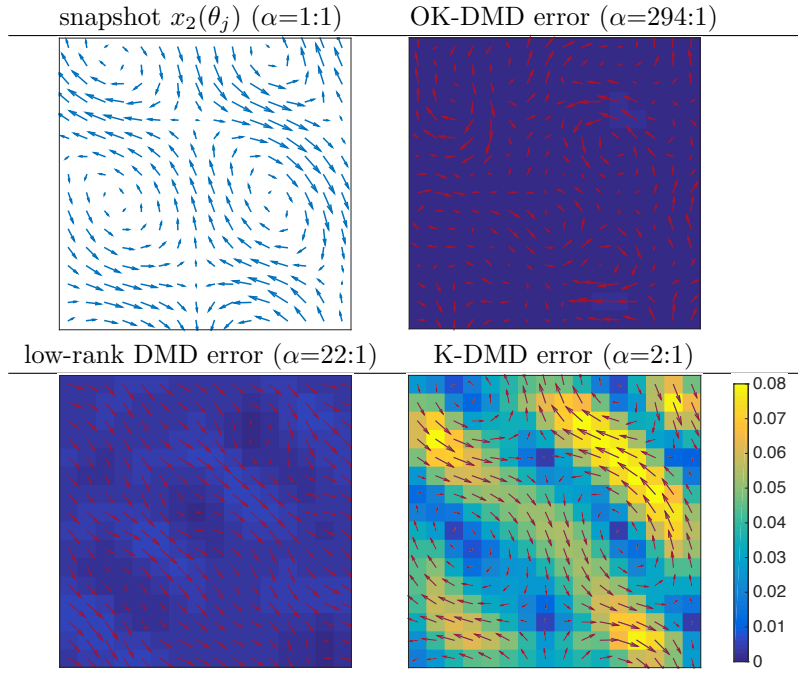


FIG. 4.3. Visualization of reduced model approximation errors. Vector field related to a snapshot  $x_2(\theta_j)$  and vector fields (enlarged at scale  $\alpha$ ) related to the approximation error  $\tilde{x}_2(\theta_j) - x_2(\theta_j)$  for  $k = 16$  superimposed on the maps of the absolute error  $|\tilde{x}_2(\theta_j) - x_2(\theta_j)|$ .